INSTITUTE OF PHYSICS PUBLISHING NONLINEARITY

Nonlinearity **18** (2005) C1–C8 doi:10.1088/0951-7715/18/1/000

COVER ILLUSTRATION

Motion and wake structure of spherical particles

Christian Veldhuis[1], **Arie Biesheuvel**[2], **Leen van Wijngaarden**[1] and **Detlef Lohse**[1,3]

[1] Department of Applied Physics, University of Twente, Enschede, The Netherlands
[2] Department of Mechanical Engineering, University of Twente, Enschede, The Netherlands

E-mail: d.lohse@utwente.nl

Received 21 October 2004
Published 13 December 2004
Online at stacks.iop.org/Non/18/C1

Abstract
This paper presents results from a flow visualization study of the wake structures behind solid spheres rising or falling freely in liquids, under the action of gravity. These show remarkable differences to the wake structures observed behind spheres held fixed. The two parameters controlling the rise or fall velocity (i.e. the Reynolds number) are the density ratio between the sphere and liquid and the Galileo number.

PACS numbers: 47.32.-y, 47.54.+r, 47.27.-i

1. Introduction

This year's cover illustration shows the boundary layer separation from a light sphere rising in quiescent water at high Reynolds number. The wake structure behind the sphere is visualized with the Schlieren technique. The experiment is part of a project to study wake structures behind falling and rising spherical particles in a large range of Reynolds numbers.

In the past years, extensive numerical investigations [1–5] have established how the wake of a sphere held *fixed* in a uniform flow undergoes a series of transitions as the Reynolds number $Re = Ud/\nu$ is increased. Here, U is the free stream velocity, d the diameter of the sphere, and ν is the kinematic viscosity of the water. It was found that the wake is axially symmetric up to $Re = 212$. Above this value, a planar-symmetric wake is found that consists of two steady counter-rotating threads. At $Re \approx 270$ there is a further transition and the planar-symmetric flow becomes time-dependent: opposite-signed streamwise vortices then form a series of loops that resemble hairpin vortices. As the Reynolds number is further increased, the flow gradually becomes more irregular and finally turbulent. The digital particle image velocimetry (DPIV) measurements by Brücker [6] and the flow visualization studies by Schouveiler and Provansal [7] have confirmed most of these numerical results and have further elucidated the sequence of transitions.

[3] Author to whom any correspondence should be addressed.

0951-7715/05/010001+08$30.00

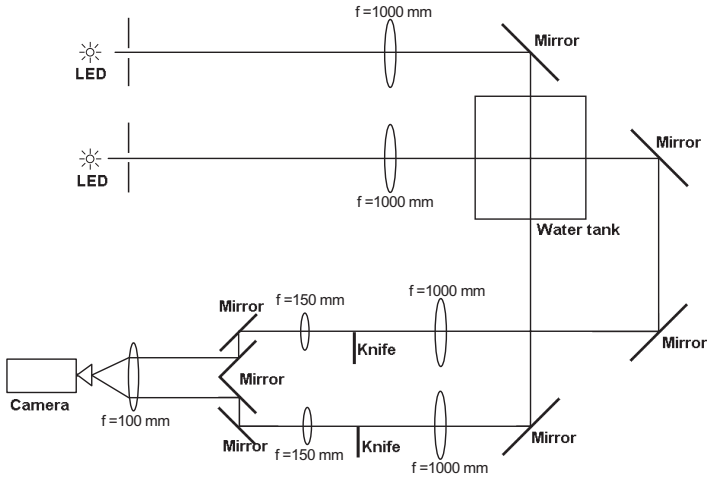

Figure 1. Top view of the Schlieren set-up used to visualize the sphere wakes.

For *freely* moving spheres the Reynolds number is defined by the measured *mean* velocity of the rise or fall of the sphere U_T and the corresponding 'Reynolds number' becomes $Re_T = \langle U_T \rangle d/\nu$. The *mean* velocity is the time-averaged velocity of the sphere, not including the acceleration of the sphere from rest. The flow loses its axial symmetry at a critical Reynolds number, which is not significantly affected by the density ratio, between solid and liquid, ρ_s/ρ [8]: $Re_{\rm cr} = 211.9$ for $\rho_s/\rho \to \infty$ (i.e. sphere held fixed), $Re_{\rm cr} = 206.3$ for $\rho_s/\rho = 0.5$ and $Re_{\rm cr} = 205.8$ for $\rho_s/\rho = 0.0$. This is in good agreement with, for example, the experimental results on solid spheres [9], on surface-contaminated gas bubbles [10], and on wake visualizations in experiments with drops of tetrachloride and chlorobenzene falling in water [11–13]. As pointed out by Natarajan and Acrivos [14], these drops must have effectively behaved as solid spheres due to the presence of surface-active impurities, and these visualizations have, therefore, often served as a basis of comparison with numerical studies on fixed spheres.

What happens for *freely* falling or rising spheres at higher Reynolds number, which is more common in multiphase flow applications? How are the wake structures and transitions observed for the fixed sphere case modified? Is there a (clear) difference in wake structure between rising and falling spheres? In this article, we present flow visualizations of the wakes behind freely moving solid spheres at large Reynolds numbers ($Re = 450$–4623) for which the density ratio ρ_s/ρ is in the range 0.50–2.63.

2. Experimental details

The flow visualizations of the sphere wakes were carried out in a transparent tank ($0.15 \times 0.15 \times 0.5\,\mathrm{m}^3$) filled with decalcified water. Smooth plastic spheres with diameters between 1.5 and 10 mm and densities between 500 and 2781 kg m^{-3} were released from rest. By means of an optical system consisting of two LED-lights, pinholes, lenses and mirrors, two perpendicular images of the particle and its wake were created and recorded at 500 frames/s with a CCD-camera (figure 1). Hence, each image consists of two perpendicular views of the same sphere. The images are taken at a position in the transparent tank where the spheres do not accelerate

Table 1. Parameter values in our visualizations; d in mm, ρ_s in kg m^{-3}. G is defined by equation (1) and Re_T is the *mean* Reynolds number ($Re_T = \langle U_T \rangle d/\langle \nu \rangle$).

	Number	d	ρ_s	$\rho_s/\langle\rho\rangle$	G	Re_T	Figure
Falling	1	3.2	1028	1.03	121	205	8
	2	4.0	1058	1.06	239	325	8
	3	1.5	2781	2.79	304	450	8
	4	6.0	1035	1.04	359	546	2
	5	6.0	1043	1.05	394	608	2
	6	4.0	2629	2.63	1261	1970	8
Rising	7	3.2	965	0.97	121	210	6
	8	5.0	950	0.95	297	450	3
	9	5.0	947	0.95	306	475	3
	10	4.0	873	0.88	334	565	6
	11	10.0	988	0.99	350	576	4
	12	8.0	982	0.99	331	602	6
	13	6.0	958	0.96	355	647	2
	14	6.0	950	0.95	390	656	2
	15	6.4	925	0.93	534	920	6
	16	6.4	864	0.87	728	1180	7
	17	7.9	925	0.93	732	1350	7
	18	6.4	650	0.65	1160	1965	7
	19	9.5	500	0.50	2548	4623	7

anymore. The wake was visualized using the Schlieren technique, which visualizes density differences due to changes in the refraction index of the fluid. To this end a small vertical temperature gradient in the water was maintained (1 K cm^{-1}). The *mean* water temperature at the measurement section was 302 K, with corresponding values of the density ($\langle\rho\rangle$) and viscosity ($\langle\nu\rangle$) of 996 kg m^{-3} and 0.802×10^{-6} m^2 s^{-1}, respectively. Hence, the Reynolds number is based on the *mean* viscosity and is defined as $Re_T = \langle U_T \rangle d/\langle\nu\rangle$. It turned out to be difficult to keep a constant temperature gradient. Therefore, the error in the *mean* water temperature at the measurement section is about 3 K, leading to a relative error in the viscosity of 10%. As opposed to the fixed-sphere problem, the Reynolds number for freely moving spheres is not an independent parameter. Following Jenny *et al* [8] we choose as independent dimensionless variables the ratio $\rho_s/\langle\rho\rangle$ of the densities and the Galileo number

$$G = \frac{(|(\rho_s/\langle\rho\rangle - 1)|g)^{1/2} d^{3/2}}{\langle\nu\rangle}. \tag{1}$$

Since $(|(\rho_s/\langle\rho\rangle - 1)|gd)^{1/2}$ can be considered as a velocity scale, G plays a similar dynamical role as the free-stream Reynolds number in the case of a fixed sphere. The parameter values for which we made the flow visualizations are summarized in table 1.

3. Observations

Figure 2 shows stereoscopic images of the wake structure behind falling spheres with densities approximately 4% (figure 2(*a*)) and 5% (figure 2(*b*)) higher than that of the surrounding liquid, and, for comparison, that behind rising spheres with densities that are approximately 4% (figure 2(*c*)) and 5% (figure 2(*d*)) lower. In all these examples, the sphere diameter is 6 mm, so that the parameter G is roughly identical in cases (*a*) and (*c*), and in cases (*b*) and (*d*). The lighter spheres have a slightly higher vertical velocity than the heavier spheres, as indicated

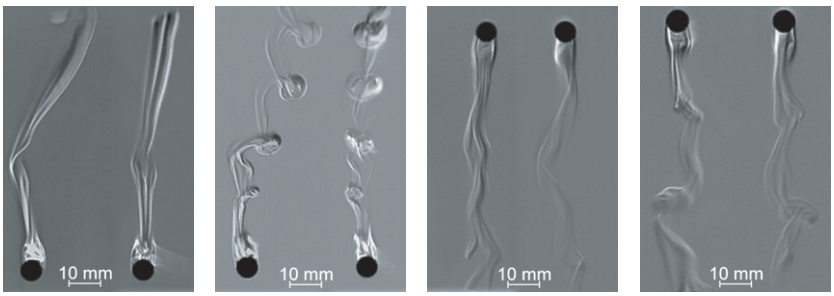

Figure 2. Stereoscopic views of falling and rising spheres and their wakes. The left part of each frame shows the xz-plane and the right part the yz-plane. In each case the sphere diameter is 6 mm. The values of the parameters $\rho_s/\langle\rho\rangle$, G and Re_T are, respectively: (*a*) 1.04, 359, 546; (*b*) 1.05, 394, 608; (*c*) 0.96, 355, 647; (*d*) 0.95, 390, 656.

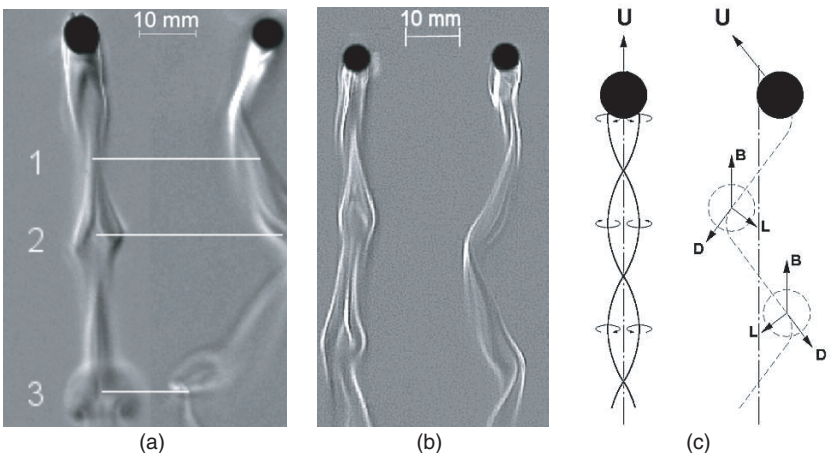

Figure 3. Stereoscopic views of rising zigzagging spheres and their wakes. The left part of each frame shows the xz-plane and the right part the yz-plane. The views illustrate the crossing at the centre-line of the zigzag path of the two counter-rotating threads of the wake ('1'), the occurrence of kinks ('2') at the extremes of the path, and the formation of hairpin-like vortices ('3') as two neighbouring kinks connect. Values of the parameters d, $\rho_s/\langle\rho\rangle$, G and Re_T are, respectively: (*a*) 5 mm, 0.95, 297, 450; (*b*) 5 mm, 0.95, 306, 475. As shown in (*c*) the crossing of the vortex threads results in a lift force L that is always directed towards the centre-line of the zigzag path. D shows the direction of the drag force and B the one of the buoyancy.

by Re_T in table 1. The wakes of the falling spheres appear to have a more 'irregular' structure, and the path followed by these spheres shows much larger deviations from a straight vertical line. These pictures illustrate that the density ratio $\rho_s/\langle\rho\rangle$ matters, even at values close to 1.

Figures 3(*a*) and (*b*) give examples of a phenomenon that we believe to be characteristic for spheres following a zigzag path, namely that the two counter-rotating threads in the wake cross at the centreline of the zigzag (indicated by '1' in figure 3(*a*)). The presence of these threads of opposite-signed streamwise vorticity implies that the sphere experiences a lift force. As a consequence of the periodic crossing of the threads this force is always directed towards the zigzag centre-line (see the sketch in figure 3(*c*)). A similar observation was made by De Vries *et al* [15] on the wake behind zigzagging gas bubbles.

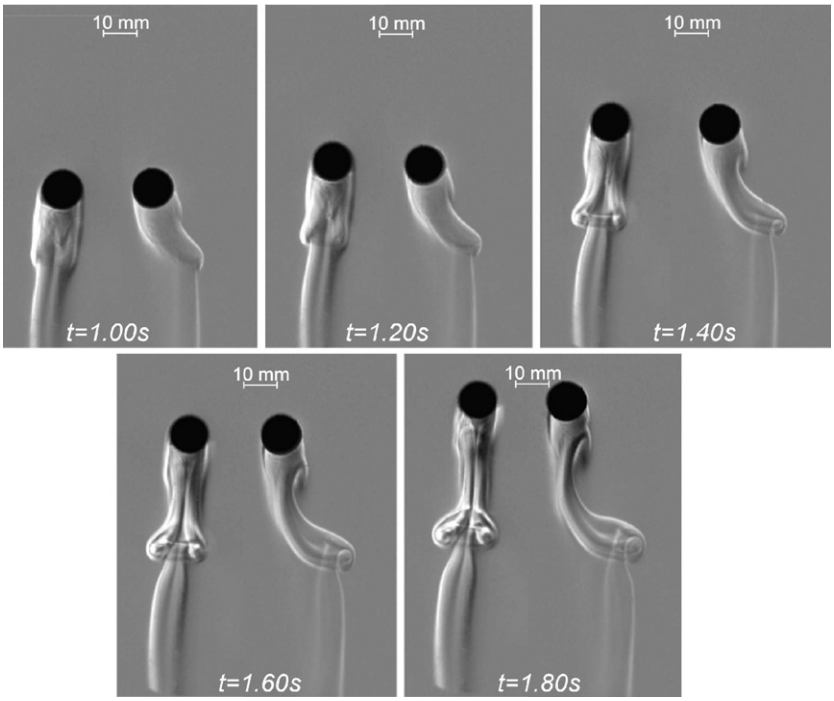

Figure 4. Sequence of stereoscopic views of a rising sphere and its wake. The left part of each frame shows the xz-plane and the right part the yz-plane. The views illustrate the process of formation of a hairpin-like vortex ($d = 10$ mm, $\rho_s/\langle\rho\rangle = 0.99$, $G = 350$ and $Re_T = 576$).

Schouveiler and Provansal [7] remark that for a fixed sphere 'the dynamics of the two opposite-sign streamwise ... vortices presents a striking similarity with the long-wavelength (or Crow) instability of a pair of counter-rotating parallel vortices' and further 'such a vortex pair instability could be responsible for the appearance of unsteadiness in the sphere wake'. Figure 3 suggests that the situation is slightly different for freely moving spheres. Here, it appears that close to the sphere each of the vortices first develop a 'kink' (indicated by '2' in figure 3(a)), a process in which the curvature of the vortices presumably plays an important role [16]. As the kinks develop further downstream of the sphere they come near each other and finally combine into what resembles a hairpin vortex (indicated by '3'). This sequence of events can be seen in the flow visualizations presented in figure 4; see also figure 6 of [11].

As the kinks develop and hairpin-like vortices are formed further downstream, a pattern results. Lunde and Perkins [17] interpreted this pattern as a series of hairpin vortices of alternating sign, shed periodically by the spheres at the extremes of the zigzag path. Our visualizations suggest instead that the streamwise vorticity produced at the surface of the sphere does not change sign; the legs of the like-signed hairpin vortices cross at the centreline of the zigzag.

Figure 2(b) is an example in which more than one kink develops in a half-period of the zigzag. We have not yet been able to determine the conditions (in terms of the parameters $\rho_s/\langle\rho\rangle$, G or Re_T) that select the number of kinks that are formed. What is remarkable is that the development of the kinks and the subsequent formation of the hairpin vortices do not seem to affect the trajectory of the sphere. This corroborates the opinion that at high Reynolds numbers the details of the vorticity distribution very close to a body basically determine the forces that it experiences.

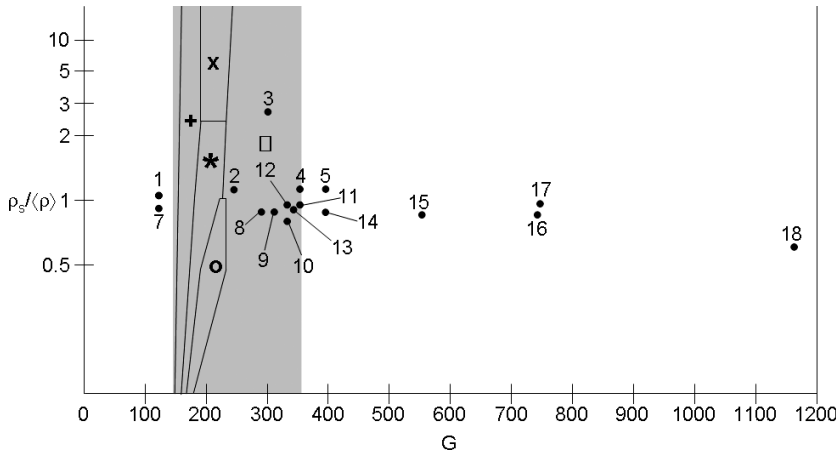

Figure 5. Phase diagram: density ratio $\rho_s/\langle\rho\rangle$ versus Galileo number. The grey box is the regime analysed by Jenny *et al* [8]. They find in the leftmost region an axisymmetric wake. The symbols, directly taken from [8], denote: + steady and oblique, $*$ oblique and oscillating regime with low frequency ($0.045 \leqslant f \leqslant 0.068$), $\times$ oblique and oscillating regime with high frequencies ($f = 0.180$), O zigzagging periodic regime ($0.023 \leqslant f \leqslant 0.035$) and □ chaotic regime. The numbers denote the number of our experiment in table 1. Experiments 6 and 19 fall outside the diagram.

We will now turn to experiments with density ratios more different from one. Recently, Jenny *et al* [18] reported on their numerical work on freely moving spheres in a Newtonian fluid. They focused on the frequencies in the wake and the path of the sphere in the parameter space spanned by the density ratio and the Galileo number. Figure 5 reproduces their phase diagram. The numbers in the diagram refer to the numbers of the experiments given in table 1. A lot of our experiments are outside their investigated region and new experiments should be done in the interesting regions around a Galileo number of 200. Further experiments should focus more on the frequencies in the wake of the sphere and compare this to the frequencies given by Jenny *et al* (see caption of figure 5). Furthermore, we must stress that wake visualizations with the Schlieren method demand a temperature gradient in the water. Hence the density and viscosity of the water are not constant through the entire flow field and the local Galileo number will not be constant. The differences between the *mean* Galileo number and the local Galileo number can reach 10% and must be taken into account when analysing figure 5.

A striking difference between our experimental data and the numerical data of Jenny *et al* is the behaviour of falling spheres with a density ratio close to one. From figures 2 and 8 it can be seen that these falling spheres can also fall in a non-vertical path. This contradicts Jenny *et al* who claim that only rising spheres can take a zigzagging path (the circles in the phase diagram figure 5).

From our experiments one concludes that for increasing Reynolds number the wake becomes more irregular (figures 6–8). The two-threaded wake structure is also present for higher Reynolds numbers. Is the double-threaded wake structure also present in the case of the highest Reynolds numbers, where the wake structure has a turbulent structure? If so, do instabilities in the wake cause kinking of the vortex threads, which leads to this turbulent wake structure? Further research will address these questions in order to get a better understanding of the boundary layer separation from spheres at high Reynolds numbers as shown on this year's cover.

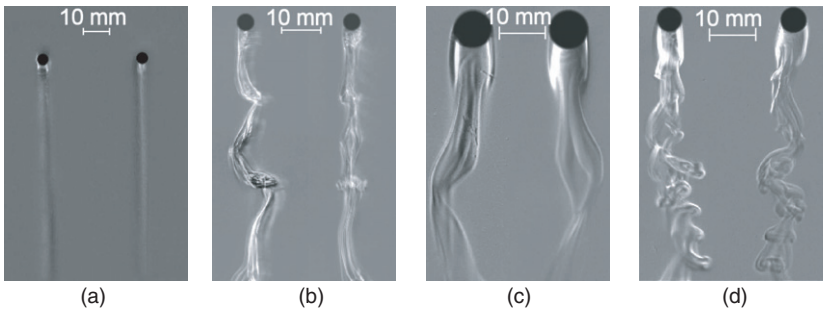

Figure 6. Stereoscopic views of rising spheres and their wake structures observed at several Reynolds numbers (Reynolds number increases from (*a*) to (*d*) and continues in figure 7). The left part of each frame shows the xz-plane and the right part the yz-plane. Values of the parameters d, $\rho_s/\langle\rho\rangle$, G and Re_T are, respectively: (*a*) 3.2 mm, 0.97, 121, 210; (*b*) 4.0 mm, 0.88, 334, 565; (*c*) 8.0 mm, 0.99, 331, 602; (*d*) 6.4 mm, 0.93, 534, 920.

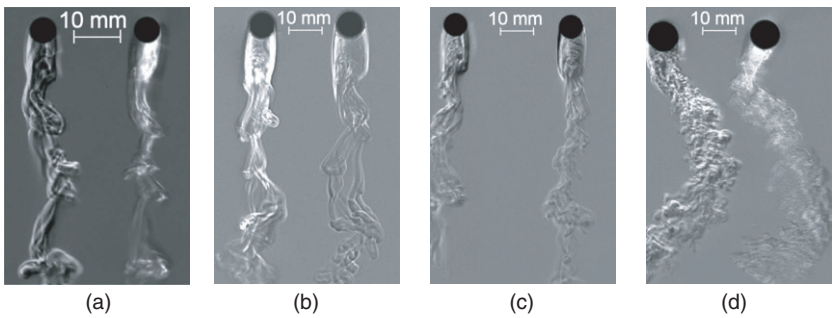

Figure 7. Stereoscopic views of rising spheres and their wake structures observed at several Reynolds numbers (Reynolds number increases from (*a*) to (*d*)). The left part of each frame shows the xz-plane and the right part the yz-plane. Values of the parameters d, $\rho_s/\langle\rho\rangle$, G and Re_T are, respectively: (*a*) 6.4 mm, 0.87, 728, 1180; (*b*) 7.9 mm, 0.93, 732, 1350; (*c*) 6.4 mm, 0.65, 1160, 1965; (*d*) 9.5 mm, 0.50, 2548, 4623.

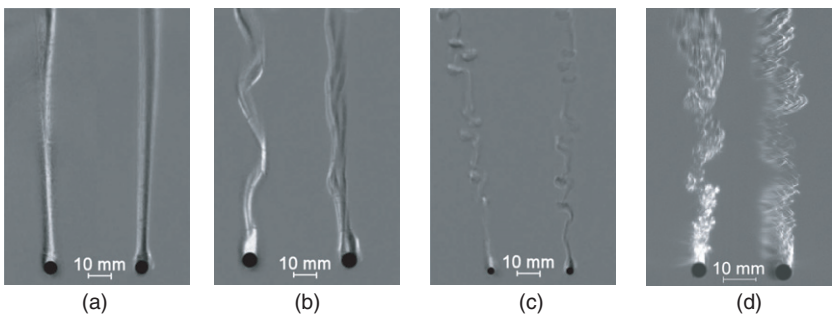

Figure 8. Stereoscopic views of falling spheres and their wake structures observed at several Reynolds numbers (Reynolds number increases from (*a*) to (*d*)). The left part of each frame shows the xz-plane and the right part the yz-plane. Values of the parameters d, $\rho_s/\langle\rho\rangle$, G and Re_T are, respectively: (*a*) 3.2 mm, 1.03, 121, 205; (*b*) 4.0 mm, 1.06, 239, 325; (*c*) 1.5 mm, 2.79, 304, 450; (*d*) 4.0 mm, 2.63, 1261, 1970.

4. Conclusions

Flow visualizations of the wakes behind solid spheres moving under the action of gravity reveal remarkable differences when compared to the wakes behind spheres held fixed: the crossing of threads of opposite-signed vorticity and the formation of kinks on these threads that develop into hairpin vortices. The ratio between the densities of the sphere and that of the surrounding fluid appears to be important. Our experiments clearly show the differences in path and wake structure between rising and falling spheres with the same Galileo number. Furthermore, the double-threaded wake structure seems to be a basic feature, even for large Reynolds numbers. This should be investigated thoroughly in future research.

Acknowledgments

The authors thank Andrea Prosperetti, M Versluis and C D Ohl for helpful discussions and suggestions and G-W Bruggert and H Scholten for the technical support. This work is part of the research programme of the Stichting voor Fundamenteel Onderzoek der Materie (FOM), which is financially supported by the Nederlandse Organisatie voor Wetenschappelijk Onderzoek (NWO).

References

[1] Johnson T A and Patel V C 1999 Flow past a sphere up to a Reynolds number of 300 *J. Fluid Mech.* **378** 19–70
[2] Lee S 2000 A numerical study of the unsteady wake behind a sphere in a uniform flow at moderate Reynolds numbers *Comput. Fluids* **29** 639–67
[3] Tomboulides A G and Orzag S A 2000 Numerical investigation of transitional and weak turbulent flow past a sphere *J. Fluid Mech.* **416** 45–73
[4] Ghidersa B and Dušek J 2000 Breaking of axisymmetry and onset of unsteadiness in the wake of a sphere *J. Fluid Mech.* **423** 33–69
[5] Ploumhans P, Winckelmans G S, Salmon J K, Leonard A and Warren M S 2002 Vortex methods for direct numerical simulation of three-dimensional bluff body flows: application to the sphere at $Re = 300$, 500, and 1000 *J. Comput. Phys.* **178** 427–63
[6] Brücker C 2001 Spatio-temporal reconstruction of vortex dynamics in axisymmetric wakes *J. Fluids Struct.* **15** 543–54
[7] Schouveiler L and Provansal M 2002 Self-sustained oscillations in the wake of a sphere *Phys. Fluids* **14** 3846–54
[8] Jenny M, Bouchet G and Dušek J 2003 Nonvertical ascension or fall of a free sphere in a Newtonian fluid *Phys. Fluids* **15** L9–12
[9] Nakamura I 1976 Steady wake behind a sphere *Phys. Fluids* **19** 5–8
[10] Hartunian R A and Sears W R 1957 On the instability of small gas bubbles moving uniformly in various liquids *J. Fluid Mech.* **3** 27–47
[11] Magarvey R H and Bishop R L 1961*a* Wakes in liquid-liquid systems *Phys. Fluids* **4** 800–5
[12] Magarvey R H and Bishop R L 1961*b* Transition ranges for three-dimensional wakes *Can. J. Phys.* **39** 1418–22
[13] Magarvey R H and MacLatchy C S 1965 Vortices in sphere wakes *Can. J. Phys.* **43** 1649–56
[14] Natarajan R and Acrivos A 1993 The instability of the steady flow past spheres and disks *J. Fluid Mech.* **254** 323–44
[15] de Vries A W G, Biesheuvel A and van Wijngaarden L 2002 Notes on the path and wake of a gas bubble rising in pure water *Int. J. Multiphase Flow* **28** 1823–35
[16] Betchov R 1965 On the curvature and torsion of an isolated vortex filament *J. Fluid Mech.* **22** 471–9
[17] Lunde K and Perkins R J 1997 Observations on wakes behind spheroidal bubbles and particles ASME-FEDSM97–3530
[18] Jenny M, Dušek J and Bouchet G 2004 Instabilities and transition of a sphere falling or ascending freely in a Newtonian fluid *J. Fluid Mech.* **508** 201–39